115th Rutgers Statistical Mechanics Conference, May 8-10, 2016:

Molecular Model for Chiral Symmetry Breaking

[20 minutes + 5 minutes for questions]

Abstract

The basic role of dominant molecular chirality in terrestrial biochemistry invites statistical mechanical modeling of how it could have initially appeared. The specific approach to be described involves a three-dimensional continuum model with flexible tetrameric molecules possessing mirror-image stable geometries. Molecular dynamics results for this model's condensed phases reveal spontaneous chiral symmetry breaking in both liquid and crystalline states.

Molecular biology clearly shows that key molecules involved in terrestrial living organisms (proteins, DNA, RNA, carbohydrates, ...) exhibit chemical structures with strongly biased handedness (chirality). It is hard to imagine how life would be possible without this geometric bias. Ultimately it is the responsibility of geology and geochemistry to decide how and why this structural preference arose on the Earth. For now it is the job of statistical mechanics to create and study possible mechanisms for chiral symmetry breaking at the molecular scale that might serve as candidates for our ancient terrestrial history. This presentation will describe one such elementary model under examination at Princeton by my collaborators and myself.

==========

View 1. Title, coauthors, affiliations, financial support.

==========

The basic molecular unit in the model is a flexible tetramer. Its two equivalent mechanically stable mirror images are illustrated in View 2.

==========

View 2. Flexible tetramer model, stable structures for isolated molecules.

==========

These involve three equal bond lengths, two 90^o bond angles, and a $\pm 90^o$ dihedral angle. It should be mentioned in passing that this geometry was suggested by, and is roughly similar to, the chiral molecular structures of the well-known 4-atom substances hydrogen peroxide H_2O_2, and its chemical

relative hydrogen disulfide H_2S_2. In our model the four monomeric units are assigned a common mass *m*.

Any deviation from the stable tetramer structures incurs an intramolecular potential energy increase, details of which are defined in the following View 3. This involves three harmonic bond stretch

==========

View 3. Tetramer intramolecular potential energy $\Phi^{(1)}$.

==========

contributions, two harmonic bond-angle bending contributions, and a dihedral angle φ deformation term with minima at $\pm 90^{o}$. This last contribution has two distinct maxima, at 0^{o} and at $\pm 180^{o}$, creating tetramer transition states . The next View 4 illustrates these two distinct planar

==========

View 4. Planar transition states for an isolated tetramer.

==========

transition states (respectively called "cis" and "trans" in conventional chemical notation). Both of these transition states have the same excitation energy K_{dih} above the stable tetramer minima.

The expression shown earlier for $\cos\varphi$ is invariant to mirror imaging, and thus as required does not distinguish opposite enantiomers. However the molecular geometry leads to a straightforward scalar measure $-1 \le \zeta \le +1$ of the chirality exhibited by a tetramer in an arbitrary state of deformation. This is defined in View 5. The mechanically stable tetramer

==========

View 5. Scalar chirality measure $\zeta(\mathbf{r}_1, \mathbf{r}_2, \mathbf{r}_3, \mathbf{r}_4)$.

==========

configurations shown earlier belong respectively to the lower and upper ζ bounds. The two distinguishable transition states each have vanishing ζ. In fact $\zeta = 0$ for all planar tetramer configurations, and that defines the multidimensional boundary between the two individually connected subspaces for the distinct chirality tetramer configurations. That is, the algebraic sign of ζ is a precise classification criterion for a tetramer's chirality. This algebraic sign assignment for every tetramer present in a condensed phase allows evaluation of its conventional "enantiomorphic excess" in terms of the numbers N_+ and N_- of tetramers possessing positive or negative ζ, respectively.

Before examining those condensed phases composed of many tetramers, it has been useful to observe the chiral inversion kinetic behavior of a single tetramer dissolved in a structureless solvent. The following View 6

==========

View 6. Monomer-solvent and solvent-solvent L-J pair interactions.

==========

indicates that the monomer-solvent and the solvent-solvent interactions are specified to be identical Lennard-Jones 12,6 pair interactions. Solvent particles are assigned the same mass m as the monomers.

Molecular dynamics calculations traditionally are performed in terms of dimensionless units. In order to maintain a sensible focus on at least part of the behavior of this model which nominally presents a significant number of distinct parameter choices, we have confined our investigation to only one specific set of dimensionless parameters. The next View 7 shows that the

==========

View 7. Dimensionless intramolecular potential energy parameters, and their scaling units.

$$[\, m = 8.5 \text{ g/mol}, \quad \varepsilon_0 = 0.15535 \text{ kcal/mol}, \quad \sigma_0 = 1.115 \text{Å} \,]$$

==========

units for scaling into dimensionless form utilize combinations of the monomer quantities $m, \varepsilon_0,$ and σ_0. View 7 also indicates what these scaling units equal in physical terms when those three monomer parameters are assigned values very roughly consistent with the molecular properties of H_2O_2 and H_2S_2. The intramolecular interaction $\Phi^{(1)}$ parameters have also been chosen to be in ranges roughly corresponding to those two molecules, with dimensionless values also displayed in View 7. In particular, the dimensionless value 17.86 shown for the tetramer's transition state barrier height K_{dih} amounts in conventional units to 2.775kcal/mol, or 0.1203eV.

With this convention, the time dependence of the dihedral angle for a single dissolved tetramer has been evaluated by molecular dynamics simulations. View 8 exhibits the results obtained at two reduced

==========

View 8. Single solvated tetramer $\varphi(t)$ plots for $T = 4.0$ and $T = 2.0$, $\rho = 0.6624$ (total L-J center density). $N_s = 4096 - 4 = 4092$.

==========

temperatures. The distributions cluster around the undeformed tetramer dihedral angles $\varphi = \pm 90^{\text{o}}$, but with thermally activated deviations, and

obvious chiral inversions through both transition state neighborhoods (0^{o} "cis", and $\pm 180^{o}$"trans"). Notice the widely different time scales used for the two plots. The net inversion rate ratio between the two temperatures is approximately 100.

Those net inversion rates can be separated into distinct contributions from the two distinguishable transition states, depending on the very different values exhibited by $\varphi(t)$ during the chirality switch. Because the downward curvatures of $\Phi^{(1)}$ (imaginary normal mode frequencies) are found to be the same for the cis and trans saddle points, the transition rates can be inferred from the corresponding transition zone tetramer probabilities. View 9

==========

View 9. Bar graphs for relative transition rates (transition zone relative populations) for the alternate pathways: "cis" *vs*. "trans".

==========

graphically displays the results for the two states just examined in the preceding View 8. The bar graphs shown are normalized for each temperature, *i.e.*, to add separately to unity for red and for blue. This shows a modest temperature-dependent effect. The cis pathway exhibits the dominant transition rate at $T = 2.0$ (by roughly a factor of 2), but increasing the temperature reduces that dominance by a modest amount.

Generating condensed phases of the tetramers for the model requires defining intermolecular interactions. We have chosen them to be pairwise additive among tetramers. As View 10 shows, these pair interactions

==========

View 10. Tetramer pair potential format.

==========

nominally are sums of 16 Lennard-Jones 12,6 potentials between monomers, one from each of the two tetramers involved. The key novel feature is that the energy coupling strength of these spherical Lennard-Jones functions is renormalized by an amount depending on the instantaneous values of the scalar chirality parameters $\zeta^{(\alpha)}$ and $\zeta^{(\gamma)}$ for the two interacting tetramers α and γ. Consequently, each inter-tetramer "L-J" interaction is actually an eight-monomer interaction function. This renormalization has a strength determined by a parameter λ that is subject to the constraint $|\lambda| < 1$. The condensed phase simulations carried out thus far have set $\lambda = 0.5$ or $\lambda = -0.5$ respectively to favor common chirality, or opposite chirality, for neighboring tetramers (at least at low to moderate pressures).

It has been well known for a long time that freezing can cause isotropic achiral molecular liquids to spontaneously form chiral crystal structures. Recent experiments [C. Dressel, *et al.*, 2014] have also demonstrated that upon cooling, certain isotropic liquids composed of nominally achiral molecules can spontaneously separate into coexisting chiral liquid phases, both of which remain isotropic. The following View 11 reproduces two

==========

View 11. Two microscope views under polarized light of coexisting pair of isotropic chiral liquids [C. Dressel, *et al.*, Nature Chem. **6**, 971-977 (2014); Institute of Chemistry, Martin-Luther Univ., Germany].

==========I

microscope images under polarized light of films of coexisting chiral liquids at $210^{o}\mathrm{C}$. These are composed of organic molecules containing 138 atoms. The relative angle set between the incident polarized beam (P) and the analyzer (A) produces distinguishable light transmissions for the two liquids. But rotation of the P-A pair at fixed relative angle between them causes no change in the relative transmission, demonstrating that both phases are isotropic liquids. Evidently intermolecular interactions can be strong enough and conformationally specific enough to produce spontaneous chiral symmetry breaking above the freezing temperature, while maintaining isotropy. This raises the possibility that our tetramer model could also generate coexisting pairs of opposite-chirality isotropic liquids. This has been tested and demonstrated in our tetramer model, with $\lambda = +0.5$ to predispose toward local enantiopurity.

At very high temperature, any such conformational bias would be overcome by strong thermal agitation. This is illustrated in View 12.

==========

View 12. $\langle \zeta(t) \rangle$ at $T = 4.0,\ \rho = 0.17,\ N_{tetr} = 1024$, enantiopure initial state.

==========

The result demonstrates that an enantiopure initial state is driven quickly toward the racemic state $\langle \zeta \rangle = 0 = ee$, around which it permanently fluctuates. But lowering the temperature isochorically within the stable liquid range produces a different scenario as shown in View 13. Now the

==========

View 13. $\langle \zeta(t) \rangle$ at $T = 2.0,\ \rho = 0.17,\ N_{tetr} = 1024$, enantiopure initial state.

==========

trend is toward a positive $\langle\zeta\rangle$ value (and thus a positive ee value) at long elapsed time, a signature of chiral symmetry breaking. It is important to note that this lower temperature trend toward spontaneous symmetry breaking has at least temporarily created coexisting slabs of opposite-chirality liquids, a phenomenon repeatedly observed in the molecular dynamics simulations. This is analogous to the experimentally observed coexisting chiral isotropic liquids whose images were shown earlier.

A similar appearance of coexisting opposite-chirality phases also arises when the initial configuration is irregular and racemic ($\langle\zeta\rangle = 0$). The next View 14 illustrates this feature occurring at a lower temperature but at the

==========

View 14. Coexisting phases appearing spontaneously from a disordered racemic initial configuration, $T = 1.4$, $\rho = 0.17$.

==========

same tetramer number density.

The interface between opposite chirality liquids has a positive surface free energy. This amounts to a long-term driving force to eliminate such interfaces, *i.e.*, to convert the system to a single chirality liquid. The following View 15 presents overall chirality evolutions for a set of 20

==========

View 15. Average chirality evolution, 20 cases, $T = 1.4$, $\rho = 0.17$, equal planar slabs of opposite chirality for initial configuration. Two cases highlighted in red for clarity.

==========

molecular dynamics runs at $T = 1.4$, each with configurationally identical starting configurations that contained equal slabs of opposite chirality. There is considerable dispersion in the results, but as the two red cases illustrate, there seems to be a tendency to evolve to average chirality about ± 0.6 . However several of the cases are still fluctuating around zero even after passage of 80,000 time units.

One naturally anticipates that the chiral liquids will undergo first-order freezing when the temperature is low enough. We have searched for the likely stable crystal structure for the $\lambda = +0.5$ case at low pressure. The search thus far indicates that the lowest energy crystal structure is indeed enantiopure. View 16 presents the results of a two-stage search, specifically

==========

View 16. Two-stage crystal structure search (simple cubic, triclinic) and their energies for $\lambda = +0.5$, $\rho_{tetr} = 0.24$. $N = 128$ tetramers. First of four equivalent layers shown, containing 32 tetramers, for both cases.

showing for clarity just the top of four equivalent layers in each case. The first stage included a constraint to simple cubic symmetry. The second stage removed that constraint, exhibiting a small reduction in energy as a result of spontaneous shear deformation from cubic into a triclinic symmetry.

Although more molecular dynamics simulations are necessary to pin down the phase changes precisely, the $\lambda = +0.5$ results available so far conform to the ee thermal equilibrium pattern indicated in View 17 for a

View 17. Schematic diagram for $ee(T)$ at fixed density approximately within the range $0.17 \le \rho \le 0.24$.

fixed moderate density. A critical temperature in the liquid range exists for appearance of the spontaneous chiral symmetry breaking. Because the chirality measure ζ is a bounded scalar quantity, this critical point may fall within the same class as that for the 3-dimensional Ising ferromagnet, thus exhibiting the same leading-order critical exponents. At fixed lower density, liquid evaporation can interfere with the pattern shown, in some circumstances eliminating the critical point, if not the entire liquid phase.

The behavior of the model under high pressure has not yet been examined. However there is one significant feature that will likely have a profound influence. This stems from the postulated renormalization property that applies to the Lennard-Jones interactions between monomers on neighboring tetramers. View 18 visually indicates the strength-modifications involved.

View 18. Chirality-renormalization effects on the L-J potential, including both its small-*r* repulsive core, and larger-*r* attractive region.

Notice the obvious energy sign reversal with respect to reducing pair distance in comparing the attractive minimum depth to the core repulsion. Although choosing $\lambda = +0.5$ biases in favor of enantiopure tetramer neighbors at low pressure (neighbor monomers near the potential minimum), it acts against that preference when high pressure forces those neighbors into significantly closer contact (neighbor monomers in the repulsive core). This will surely produce a pressure dependence of the structure of the low temperature crystal. Of course an analogous reversal phenomenon applies to the $\lambda = -0.5$ case. For both λ choices, high pressure can apparently induce enantiopure *vs*. racemic inversion.

A lot of additional numerical work needs to be devoted to refining and extending properties of the elementary tetramer model described. But additionally, other distinctive 3-dimensional continuum models for spontaneous symmetry breaking deserve also to be created and examined. In particular it would be scientifically informative to examine chiral symmetry breaking possibilities when achiral reactants are present that can form chiral product molecules via chemical bonding, in the presence of autocatalysis and heteroinhibition. This broadened context should assist the geological/geochemical community in ultimately reconstructing the detailed early history of earth's evolution.

Molecular Model for Chiral Symmetry Breaking

Folarin B. Latinwo and Pablo G. Debenedetti,

Department of Chemical and Biological Engineering,
Princeton University;

and

Frank H. Stillinger,

Department of Chemistry, Princeton University

Financial support:
National Science Foundation Grant No. CHE-1213343

View 2

Back

Flexible Tetramer Model, Stable Structures

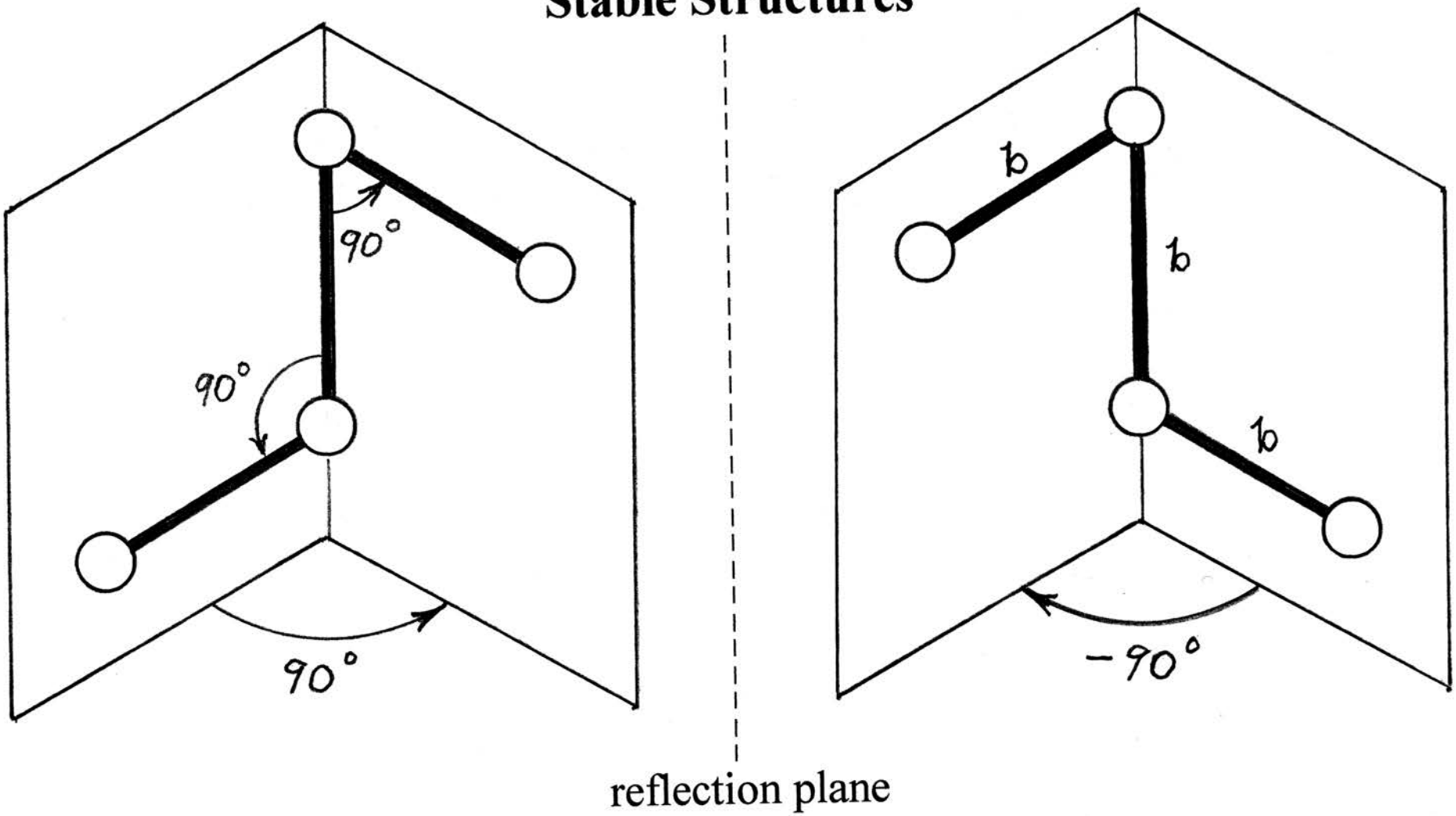

View 3

Tetramer Intramolecular Potential Energy

Back

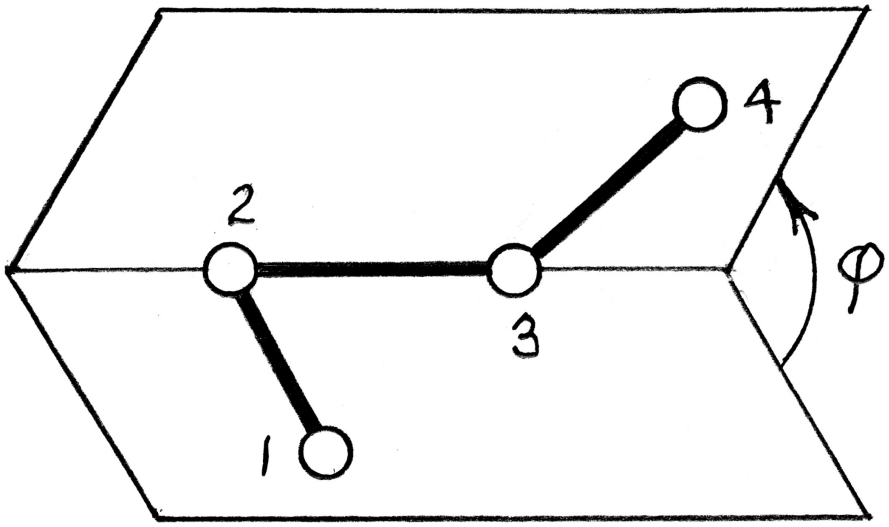

$$\Phi^{(1)}(\mathbf{r}_1,\mathbf{r}_2,\mathbf{r}_3,\mathbf{r}_4) = \sum_{i=1}^{3}(K_{str}/2)(r_{i,i+1}-b)^2 + \sum_{i=2}^{3}(K_{bnd}/2)(\theta_i-\pi/2)^2 + K_{dih}\cos^2\varphi \quad .$$

Dihedral angle $-\pi \le \varphi \le \pi$ definition:

$$\cos\varphi = \frac{(\mathbf{r}_{12}\times\mathbf{r}_{23})\cdot(\mathbf{r}_{23}\times\mathbf{r}_{34})}{|\mathbf{r}_{12}\times\mathbf{r}_{23}||\mathbf{r}_{23}\times\mathbf{r}_{34}|} \quad .$$

Distinct Planar Transition States, Isolated Tetramer

- $\varphi = 0$:

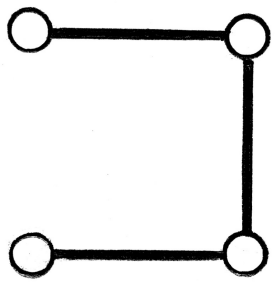

- $\varphi = \pm\pi$:

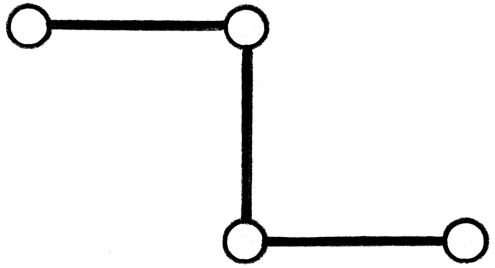

- Transition state barrier height: K_{dih}

- Harmonic normal mode frequencies at each transition state:
  five positive, six vanishing, one imaginary (reaction path)

Chirality Measure for Individual Tetramers

- Monomers located at $\mathbf{r}_1, \mathbf{r}_2, \mathbf{r}_3, \mathbf{r}_4$.
- $\zeta(\mathbf{r}_1,\mathbf{r}_2,\mathbf{r}_3,\mathbf{r}_4) = \dfrac{\mathbf{r}_{12}\cdot(\mathbf{r}_{23}\times\mathbf{r}_{34})}{|\mathbf{r}_{12}||\mathbf{r}_{23}||\mathbf{r}_{34}|} \equiv \dfrac{\mathbf{r}_{43}\cdot(\mathbf{r}_{32}\times\mathbf{r}_{21})}{|\mathbf{r}_{43}||\mathbf{r}_{32}||\mathbf{r}_{21}|}$.
- $-1 \le \zeta \le +1$; $\zeta = \pm 1$ at the $\Phi^{(1)}$ minima .
- $\zeta = 0$ for tetramer planar configurations, including the ideal transition states.
- Enantiomeric excess ("ee"): $-1 \le (N_+ - N_-)/(N_+ + N_-) \le +1$

Simple Achiral Solvent for Tetramers

- Lennard-Jones 12,6 pair potentials are postulated for monomer-solvent and for solvent-solvent interactions:

  monomer-solvent: $\varepsilon_{ms} \mathrm{v}_{\mathrm{LJ}}(r/\sigma_{ms})$ (ζ-independent) ,

  solvent-solvent: $\varepsilon_{ss} \mathrm{v}_{\mathrm{LJ}}(r/\sigma_{ss})$.

- Additional simplifications: $\varepsilon_{ms} = \varepsilon_{ss} = \varepsilon_0$, and $\sigma_{ms} = \sigma_{ss} = \sigma_0$, so that all L-J pair potentials involving solvent are identical.

Parameter Choice, Reduced Units

Back

- Elementary parameter set choice: m, ε_0, σ_0
  $[m = 8.5\text{g/mol};\quad \varepsilon_0 = 0.15535\text{kcal/mol};\quad \sigma_0 = 1.115\,\text{Å}]$

- Time unit: $\sigma_0 (m/\varepsilon_0)^{1/2}$ $\qquad [\rightarrow 0.4033\,\text{ps}\,]$

- Number density unit: σ_0^{-3} $\qquad [\rightarrow 0.7214\,\text{Å}^{-3} = 1198\,\text{mol/l}\,]$

- Temperature unit: ε_0 / k_B $\qquad [\rightarrow 78.15\,\text{K}\,]$

- Pressure unit: $\varepsilon_0 / \sigma_0^3$ $\qquad [\rightarrow 7786\,\text{bar}\,]$

- Dimensionless intramolecular ($\Phi^{(1)}$) parameters:

$$K_{str} = 8003, \quad K_{bnd} = 643.7, \quad K_{dih} = 17.86, \quad b = 1.0583$$

Inter-conversion of a single tetramer in a Lennard Jones fluid

(reduced number density = 0.6624)

T = 4.0

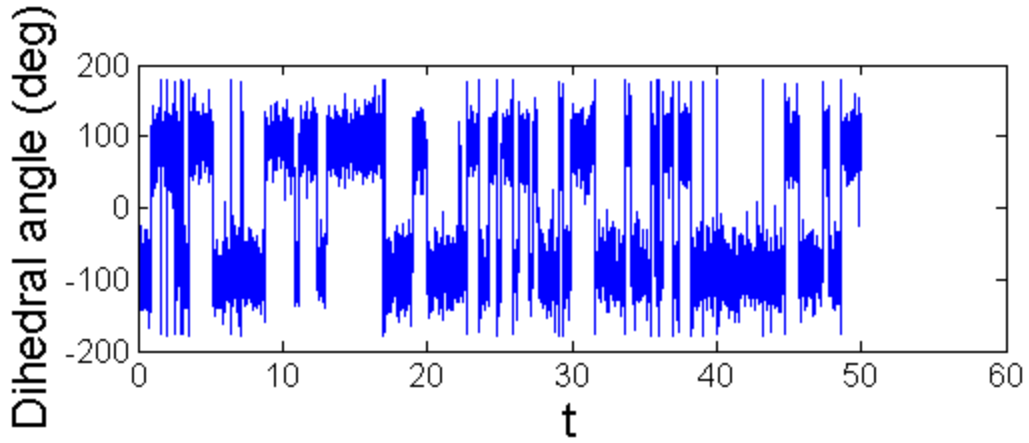

T = 2.0

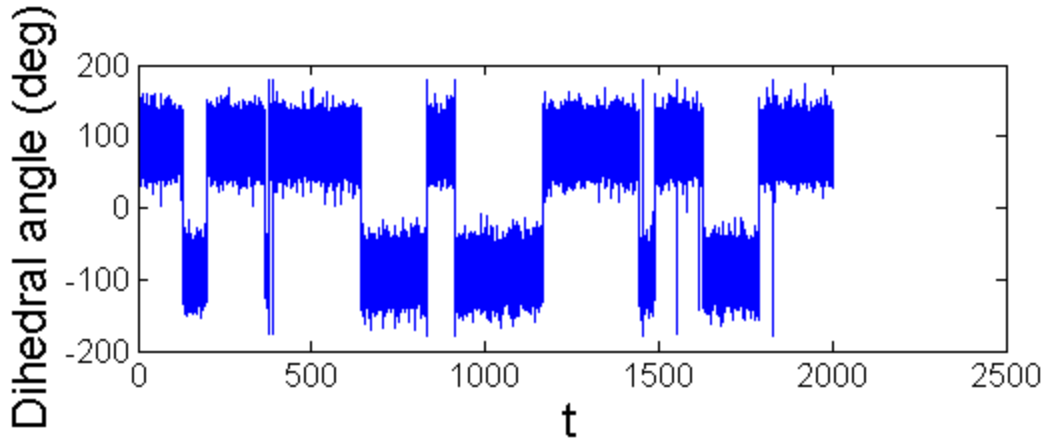

Resolved Transition Rates for the Transition States (reduced number density = 0.6624)

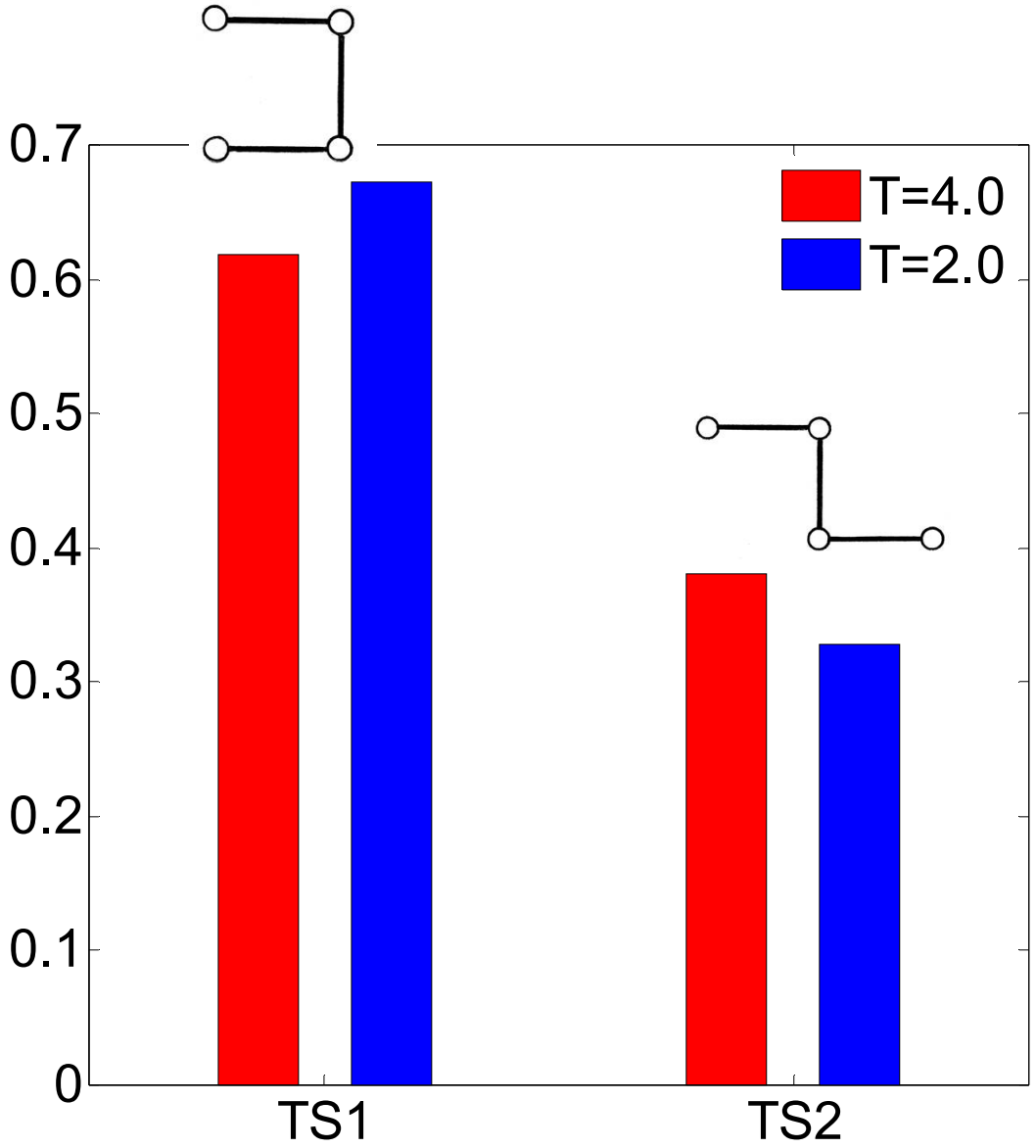

Tetramer Pair Interaction ($\Phi^{(2)}$)

- Sixteen energy-scaled Lennard-Jones pair interactions between monomers belonging to different tetramers (α, γ):

$$\Phi^{(2)} = \sum_{i=1}^{4}\sum_{j=1}^{4}\varepsilon_{mm}(\zeta^{(\alpha)},\zeta^{(\gamma)})\,\mathrm{v}_{\mathrm{LJ}}(|\,\mathbf{r}_i^{(\alpha)} - \mathbf{r}_j^{(\gamma)}\,|/\sigma_0) \quad .$$

- $\mathrm{v}_{\mathrm{LJ}}(x) = 4(x^{-12} - x^{-6})$.
- $\varepsilon_{mm}(\zeta^{(\alpha)},\zeta^{(\gamma)}) = \varepsilon_0(1+\lambda\zeta^{(\alpha)}\zeta^{(\gamma)})$, where $|\lambda| < 1$.
- $\lambda > 0$ favors like enantiomers, $\lambda < 0$ favors opposite enantiomers.
- ε_{mm} varies smoothly as the tetramers deform, passing through ε_0 when one tetramer changes chirality.

View 11

Back

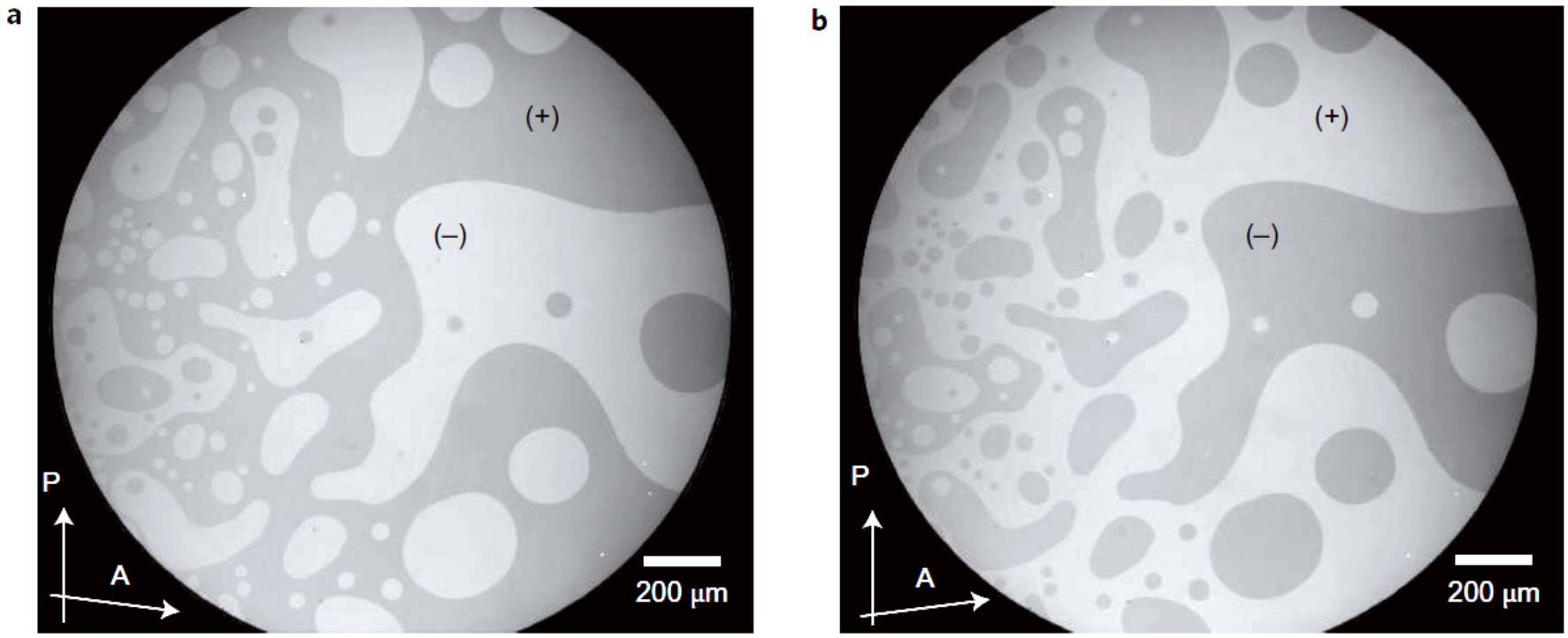

Time dependence of average chirality at high temperature, T= 4.0

(reduced tetramer number density = 0.17)

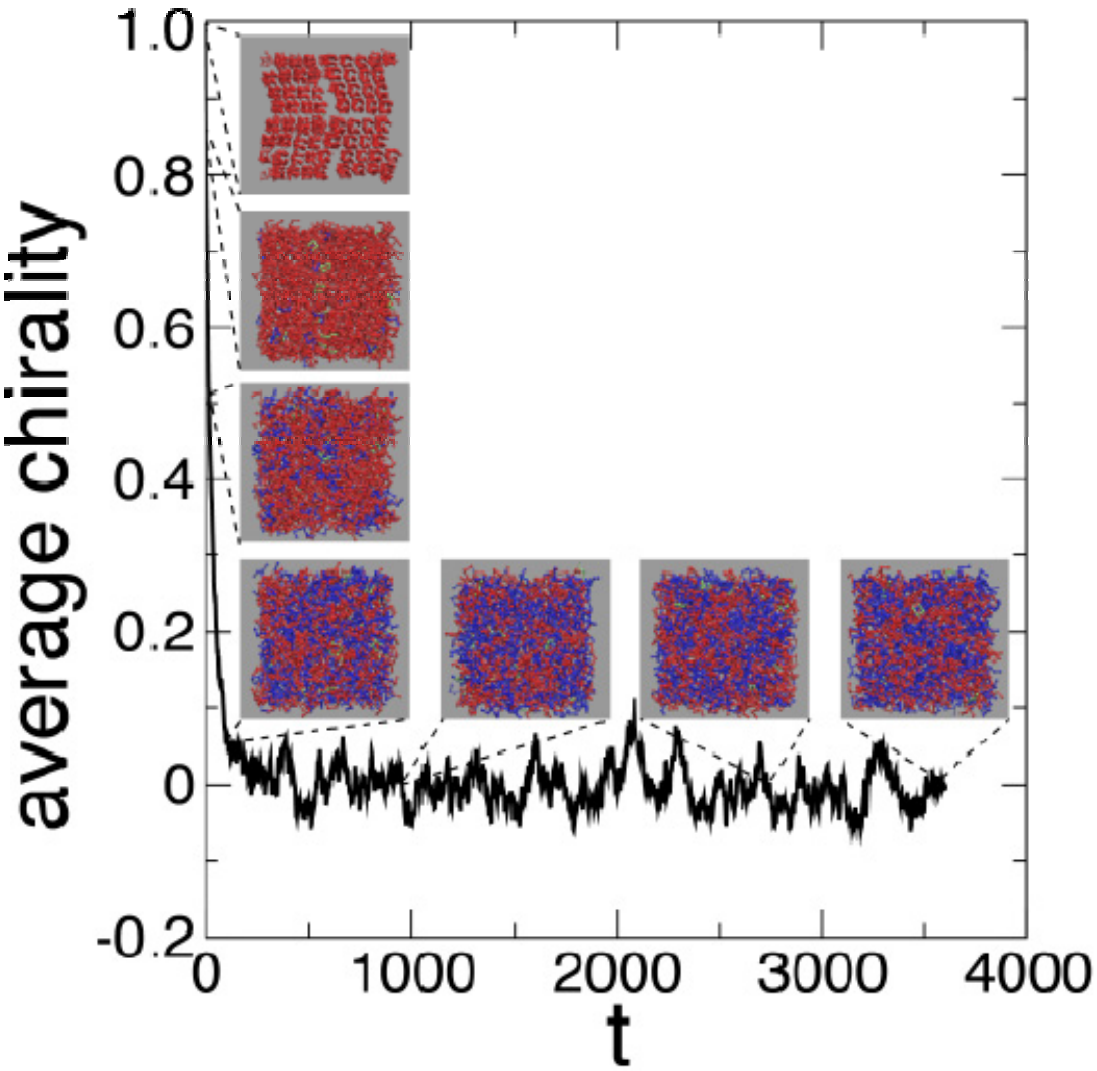

Time dependence of average chirality at high temperature, T= 2.0

(reduced tetramer number density = 0.17)

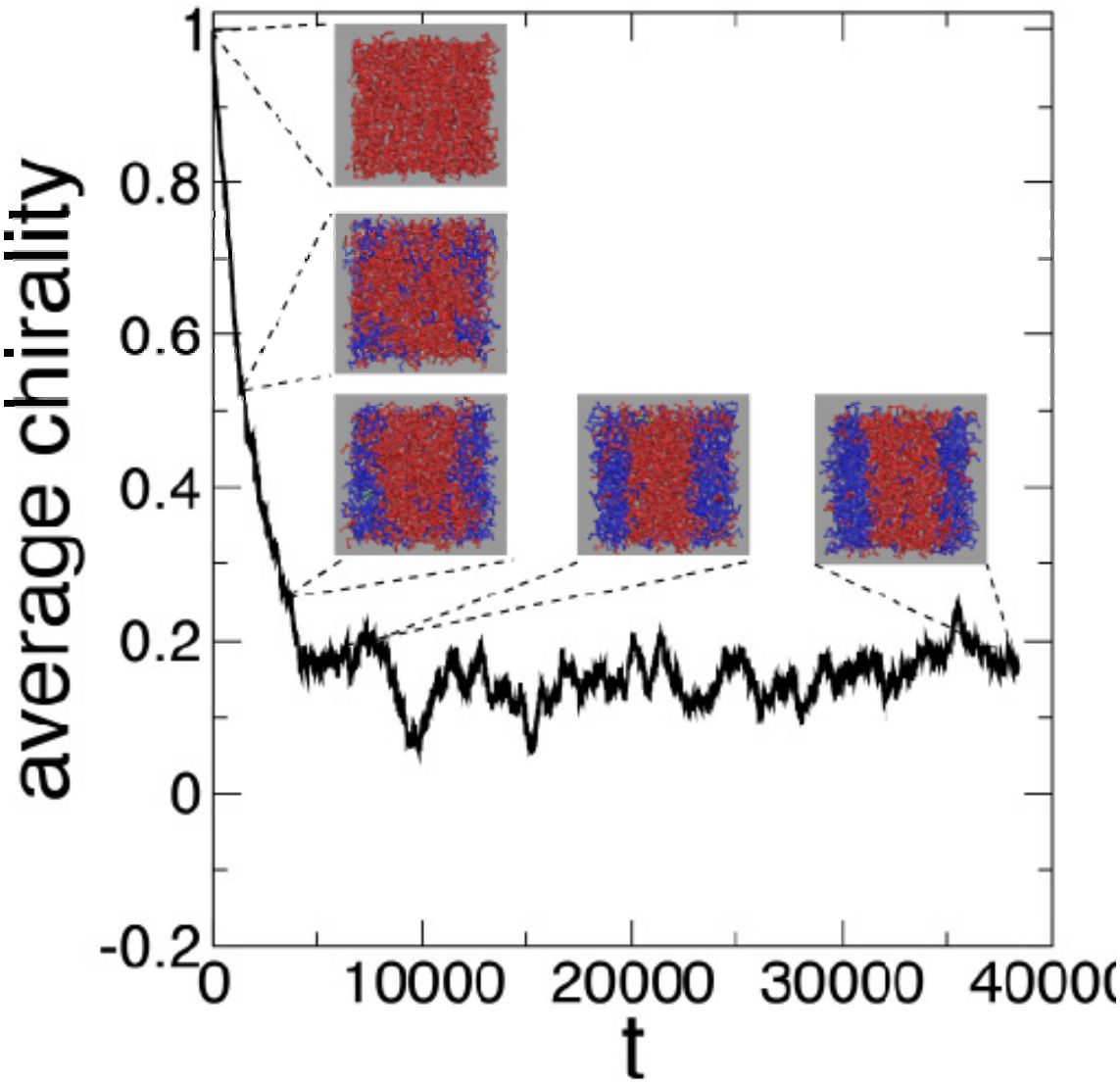

Chirality-induced liquid-liquid phase separation

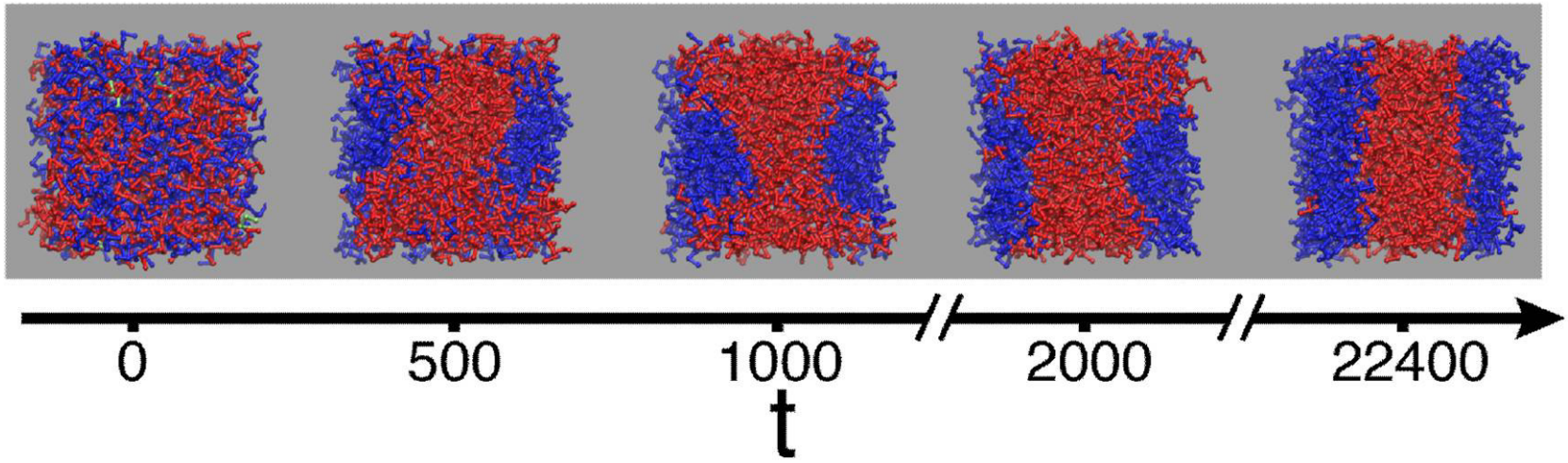

(T=1.4, tetramer number density = 0.17)

Average chirality at low temperature, T= 1.4

(reduced tetramer number density = 0.17)

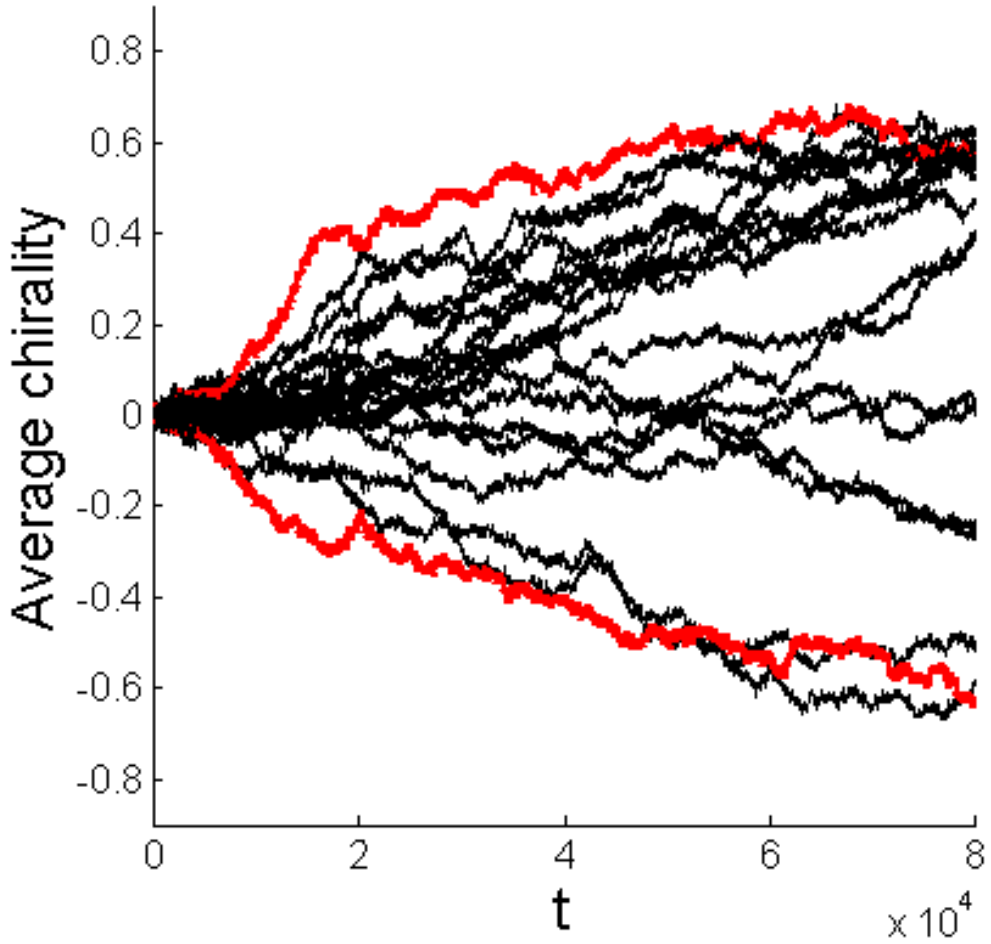

Allowing for a triclinic cell

Back

Simple cubic crystal, T= 0.01
(128 tetramers)

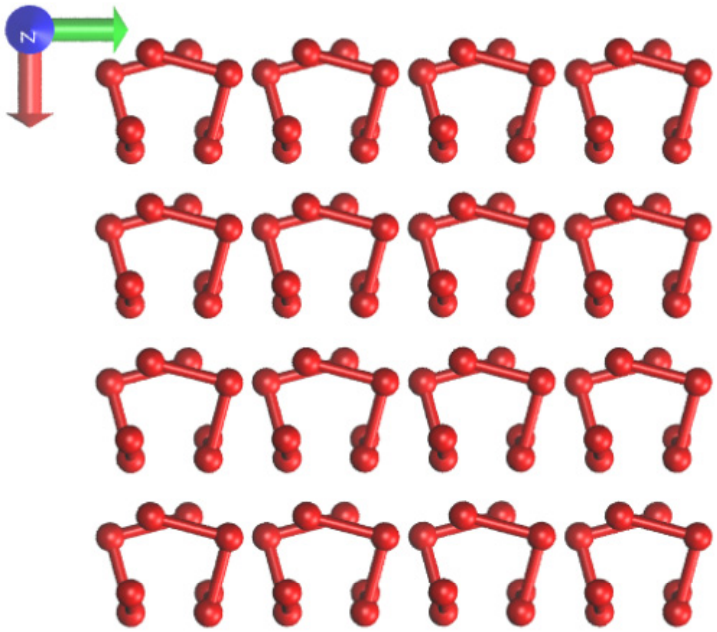

$\Phi / N_{tetr} = -29.1$

$\rho_{tetr} = 0.24$

Triclinic crystal, T= 0.01
(128 tetramers)

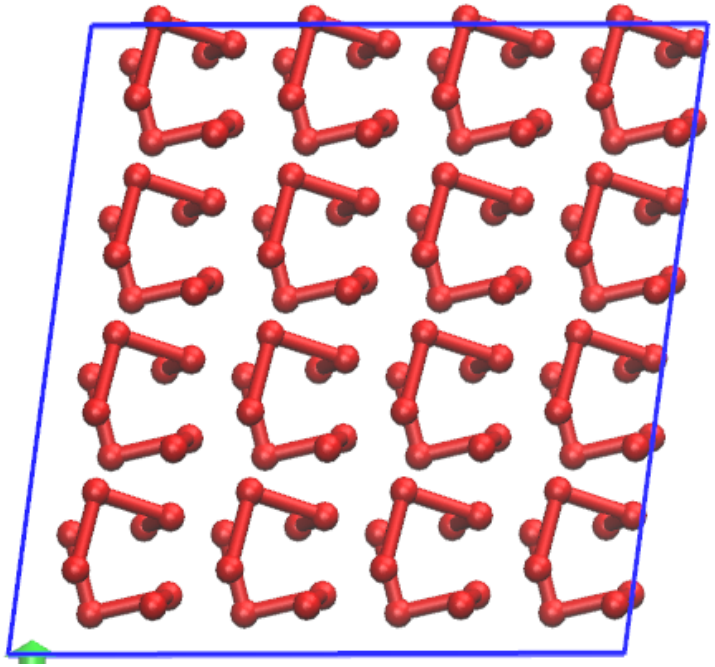

$\Phi / N_{tetr} = -29.4$

$\rho_{tetr} = 0.24$

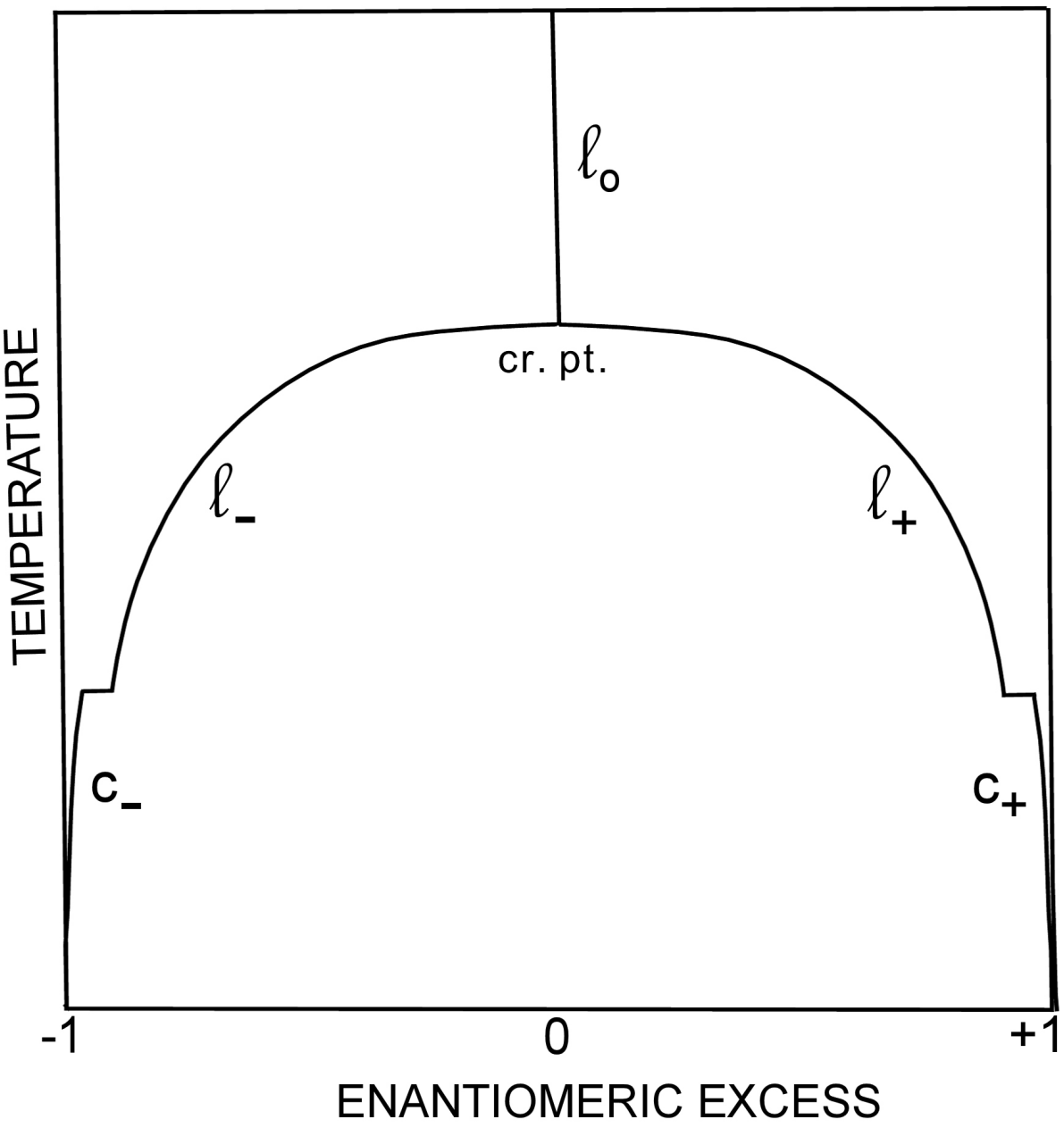
TEMPERATURE
ℓ_o
cr. pt.
ℓ_-
ℓ_+
c_-
c_+
-1
0
+1
ENANTIOMERIC EXCESS

Chirality-renormalized pair potential